Lamellar ionenes with highly dissociative, anionic channels provide lower barriers for cation transport

Michael A. Stolberg,[1,2] Benjamin A. Paren,[3] Pablo A. Leon,[2] Christopher M. Brown,[1] Gavin Winter,[2] Kiarash Gordiz,[4] Alberto Concellón,[1] Rafael Gómez-Bombarelli,[2] Yang Shao-Horn,[2,3,4,*] and Jeremiah A. Johnson[1,*]

[1]Department of Chemistry, Massachusetts Institute of Technology, 77 Massachusetts Avenue, Cambridge, Massachusetts 02139, United States.

[2]Department of Materials Science and Engineering, Massachusetts Institute of Technology, 77 Massachusetts Avenue, Cambridge, Massachusetts 02139, United States.

[3]Research Laboratory of Electronics, Massachusetts Institute of Technology, 77 Massachusetts Avenue, Cambridge, Massachusetts 02139, United States.

[4]Department of Mechanical Engineering, Massachusetts Institute of Technology, 77 Massachusetts Avenue, Cambridge, Massachusetts 02139, United States.

*Corresponding Authors, address all correspondence to: jaj2109@mit.edu & shaohorn@mit.edu

Abstract:

Solid polymer electrolytes have the potential to enable safer and more energy dense batteries; however, a deeper understanding of their ion conduction mechanisms, and how they can be optimized by rational molecular design, is needed to realize this goal. Here, we investigate the impact of anion dissociation energy on ion conduction in solid polymer electrolytes via a novel class of ionenes prepared using acyclic diene metathesis polymerization of highly dissociative, liquid crystalline fluorinated aryl sulfonimide-tagged ("FAST") anion monomers. These polyanions with various cations (Li^+, Na^+, K^+, and Cs^+) form well-ordered lamellae that are thermally stable up to 180 °C and feature domain spacings that correlate with cation size, providing channels lined with dissociative FAST anions. Electrochemical impedance spectroscopy (EIS) and differential scanning calorimetry (DSC) experiments, along with nudged elastic band (NEB) calculations, suggest that cation motion in these materials operates via an ion hopping mechanism. The activation energy for Li^+ conduction is 59 kJ/mol, which is amongst the lowest for systems that are proposed to operate via an ion conduction mechanism that is decoupling from polymer segmental motion. Moreover, the addition of a 1 equivalent of a cation-coordinating solvent to these materials led to a >1000-fold increase in ionic conductivity without detectable disruption of the lamellar structure, suggestion selective solvation of the lamellar ion channels. This work demonstrates that molecular design can facilitate controlled formation of dissociative anionic channels that translate to significant enhancements in ion conduction in solid polymer electrolytes.

Introduction. Solid polymer electrolytes (SPEs) have been studied since the early 1980s as a promising alternative to conventional liquid electrolytes for next-generation batteries.[1,2] SPEs composed of high molecular weight polymers (typically > 5,000 g/mol) have nearly zero vapor pressure and much higher autoignition points than common liquid electrolytes, rendering them potentially safer.[2] A sub-class of solid polymer electrolytes referred to as single ion conducting (SIC) polymers feature anionic groups within the polymer sidechains (i.e., ionomers) or backbones (i.e., ionenes).[3] SIC SPEs often display higher cation transference numbers (the fraction of charge carried by the cations), than conventional SPEs, which can increase battery power,[4,5] and suppress dendrite growth.[6] Nevertheless, dry SIC SPEs typically show low ionic conductivities due to their large energy barriers for polymer segmental motion and/or cation dissociation. As a result, liquid solvents[7,8] or poly(ethylene oxide) (PEO)[9,10] are often incorporated into SIC polymers to facilitate ion conduction via cation solvation, though such strategies remain limited by inherently slow polymer segmental relaxation (in the case of PEO blending)[11] or they may reduce electrolyte stability/safety (in the case of solvent addition).[3,12]

Inspired by the high ionic conductivities of solid ceramic ion conductors such as the Lithium Super Ionic Conductor (LISICON) family,[13] recent SPE designs have sought to exploit an "ion-hopping" or "decoupled" mechanism, wherein cations move between relatively stationary anionic sites at rates that are decoupled from polymer segmental relaxation,[11] the latter of which is inherently unable to provide cation mobility on par with ceramics and liquids.[14] Decoupled ion conduction is thought to be favored in materials that possess crystalline and/or highly-ordered, rigid anionic channels. For example, Winey and coworkers have suggested that decoupled ion transport occurs in SICs derived from carboxylate- or sulfonate-terminated alkanes that form lamellar and hexagonal phases (Figure 1A, **1** and **2**), respectively, driven by the crystallization of their long alkyl segments.[15,16] Sidechain-functionalized polymers with percolated ionic aggregates (**3**),[17] mesogenic sidechains that promoted nanoscale ordering (**4**),[18] or precisely placed dissociative ions (**5**)[19] have also been proposed to leverage decoupled ion conduction.[17,19,20] Nevertheless, the ion conductivities in the dry state for these materials are either low (much lower than traditional SPEs) or not reported; new design strategies are needed to facilitate cation mobility in crystalline, polyanion-based materials.

The previously reported decoupled SPEs tend to use anionic groups (e.g., carboxylates and sulfonates) that are more Lewis basic, i.e., less dissociative, than common anions used in battery electrolytes such as bis(trifluoromethanesulfonyl)imide (TFSI, **7**).[21] Even when softer, more dissociative anions such as sulfonimides are employed for polyanion designs, the linkers required to conjugate these anions to

polymers tends to involve replacing at least one strongly electron withdrawing group, e.g., CF_3, with alkyl or aryl substituents, which leads to comparably more Lewis basic anions (e.g., **5** and **6**).[9,19] We hypothesized that the cation-anion association energy, i.e., the energy required to remove a cation from its corresponding anion, may be a useful descriptor to guide SPE design, as cation hopping requires dissociation from the polymer backbone and movement to an adjacent anionic site. To quantify the impacts of anion choice, we used density functional theory (DFT) calculations to compare the association energies of a Li^+ cation and various small-molecule analogs of commonly employed polyanions in implicit *N,N*-dimethylformamide (DMF) solvent (Figure 1B and Figure S1). As expected, the carboxylate and sulfonate anions (analogous to **1**-**4**) have the most negative (i.e., more favorable) association energies, and thus they are the least dissociative. Similarly, while sulfonimide derivatives analogous to **5** and **6** are indeed more dissociative than **1**–**4**, their electron rich substituents make them less dissociative than TFSI (**7**).

Guided by the hypothesis than lowering anion dissociation energy may lower the barrier to ion hopping in SPEs, we set out to design a new class of highly ordered, ionenes[22] with chemically tunable and dissociative anionic backbones derived from bis-pentafluorophenyl sulfonimide anions ("**FAST-C"**, Figure 1C).[23] Due to its strongly electron withdrawing pentafluorophenyl substituents, **FAST-C** features an association energy (−82 kJ/mol) more similar to that of TFSI (**7**) (−84 kJ/mol) than **1**–**6**. Moreover, nucleophilic aromatic substitution (S_NAr) of the *para*-positions of **FAST-C** with thiols is expected to have a minimal effect on its association energy (the Hammett parameters for *para*-thioether and *para*-fluorine are both ~0).[24]

Single-crystal X-ray structural analysis of the **FAST-C** Na^+ salt (Figure 1D) shows that it forms channels lined with anionic sulfonamides filled with Na^+ cations in the solid state, which could facilitate ion hopping if translated to SPEs. Guided by these considerations we targeted an ionene structure in which **FAST-C** anions are evenly spaced within a poly-alkenyl backbone to promote formation of ionic channels. We report here the synthesis of a new class of highly dissociative ionene SPEs—**pFAST-C20-M** (where is M = Li^+, Na^+, K^+, or Cs^+)—prepared from acyclic diene metathesis (ADMET) polymerization of liquid-crystalline, -alkenyl-terminated, thioether functionalized monomer **FAST-C20**. **PFAST-C20-M** polymers display semicrystalline, lamellar solid-state structures with cation-size-dependent channels lined with **FAST-C**-based anions. These materials display record low activation energies and amongst the highest overall ionic conductivities for ordered, solvent-free polyanion SPEs. Moreover, the addition of 25 wt. % (1 equiv to cation) of a cation-coordinating solvent (tetraglyme) boosted ionic conductivity in these materials by 3

orders-of-magnitude without disrupting their semicrystalline lamellar morphology. These results should drive the development of novel ionenes and related SPEs based on highly dissociative anions, which may contribute to the realization of optimal decoupled SIC SPEs in the future.

A.

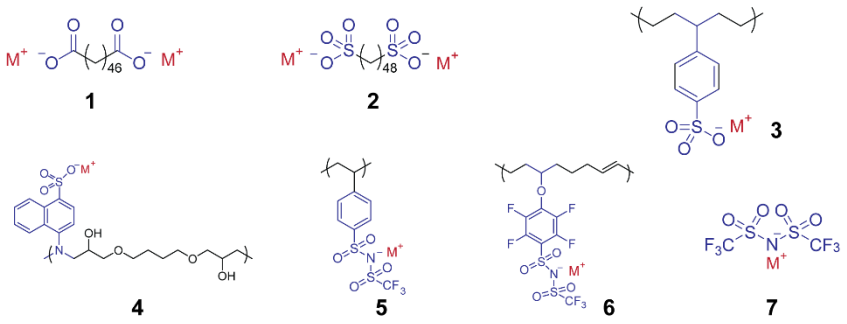

B.

Reference	+/- Solvent or Ethylene Oxide	DFT Association Energy in DMF* (kJ/mol)
1. Yan L. *et. Al.* ; 2019[14]	-	-159.3
2. Paren B. A. *et. Al.* ; 2022[15]	-	-120.6
3. Paren B. A. *et. Al.* ; 2020[18]	-	-110.5
4. Bresser D. *et. Al.* ; 2021[16]	+	-109.0
5. Stacy E. W. *et. Al.* ; 2018[17]	-	-107.45
6. Zhang W. *et. Al.* ; 2021[7]	+	-91.0
7. M-TFSI	-	-84.4
FAST-C	-	-82.4

Increasing Dissociativity

C. **This work**

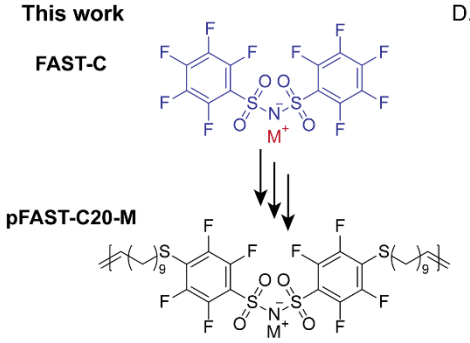

D. **FAST-C** Na Crystal Structure

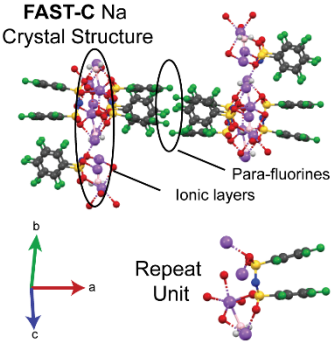

Figure 1. A) Structures of reported SPEs proposed to operate via decoupled ion transport. The portions highlighted in blue indicate the fragments that were used for DFT calculations. B) Association energies, as calculated by DFT, for model anions based on reported SPEs (**1**–**6**) for comparison to **TFSI** and **FAST-C** anions. Here, a less negative value indicates a less stable salt complex, i.e., a greater extent of dissociation. (* = implicit solvent) C) Installation of terminal alkenes onto **FAST-C** via S_NAr enabled polymerization via ADMET to form a family of ionenes **pFAST-C20-M** with different cations M. The polymer structure is designed to promote the formation of highly ordered channels

for ion hopping. D) Single crystal X-ray diffraction structure for the **FAST-C** Na^+ salt, highlighting the layers of sodium cations and anionic channels. The *para*-fluorine atoms, which are linked together through alkenyl chains in **pFAST-C20-M** polymers, are aligned in parallel. Here a ball and stick model is used; see Figure S2 for the structure shown as thermal ellipsoids.

Results and Discussion

Design and synthesis of FAST-C20 monomer. We targeted monomer **FAST-C20** (Figure 2A), which features (1) two alkene substituents for polymerization via ADMET; (2) long alkenyl chains to drive polymer crystallization;[25,26] and (3) highly dissociative thioether-linked **FAST-C** anions.[24] Heating **FAST-C** (1 equiv) and 10-undecene-1-thiol (2.2 equiv) at 80 °C in the presence of triethylamine (4 equiv) for 12 h provided **FAST-C20** as a waxy solid in 62% isolated yield on the 5 g scale following purification (Figure 2A, see supporting information for full synthetic details). ^{19}F NMR spectroscopy (Figure 2B) supported the symmetrical structure of **FAST-C20**, showing 2 peaks corresponding to the 2 sets of 4 equivalent F atoms on each side of the FAST anion, in contrast to the 3 distinct sets of F atoms on **FAST-C**. Variable-temperature small angle X-ray scattering (VT-SAXS) was used to investigate the bulk structure of **FAST-C20** (Figure 2C). At room temperature, a broad feature located at q = 0.15 $Å^{-1}$ was observed along with higher order reflections located at $2q$, $3q$, and $4q$ (Figure S4), which are indicative of a lamellar structure with a d-spacing of $d = {}^{2\pi}/_{q} = 41.9$ Å. Upon heating to 80 °C, a series of peaks assigned to a face centered cubic (FCC) structure was observed with the lattice parameter a = 61.86 Å (Figure S5). We hypothesize that the molecules form conic sections or wedges, which self-assemble into micellar structures on an FCC lattice.[27–29] Further heating to 130 °C gave overlapping broad and sharp peaks with a domain spacing of 29.9 Å, suggesting a mixture of ordered and isotropic/disordered morphologies; further heating to 180 °C produced only a broad peak at d = 28.55 Å indicative of an isotropic/disordered phase.

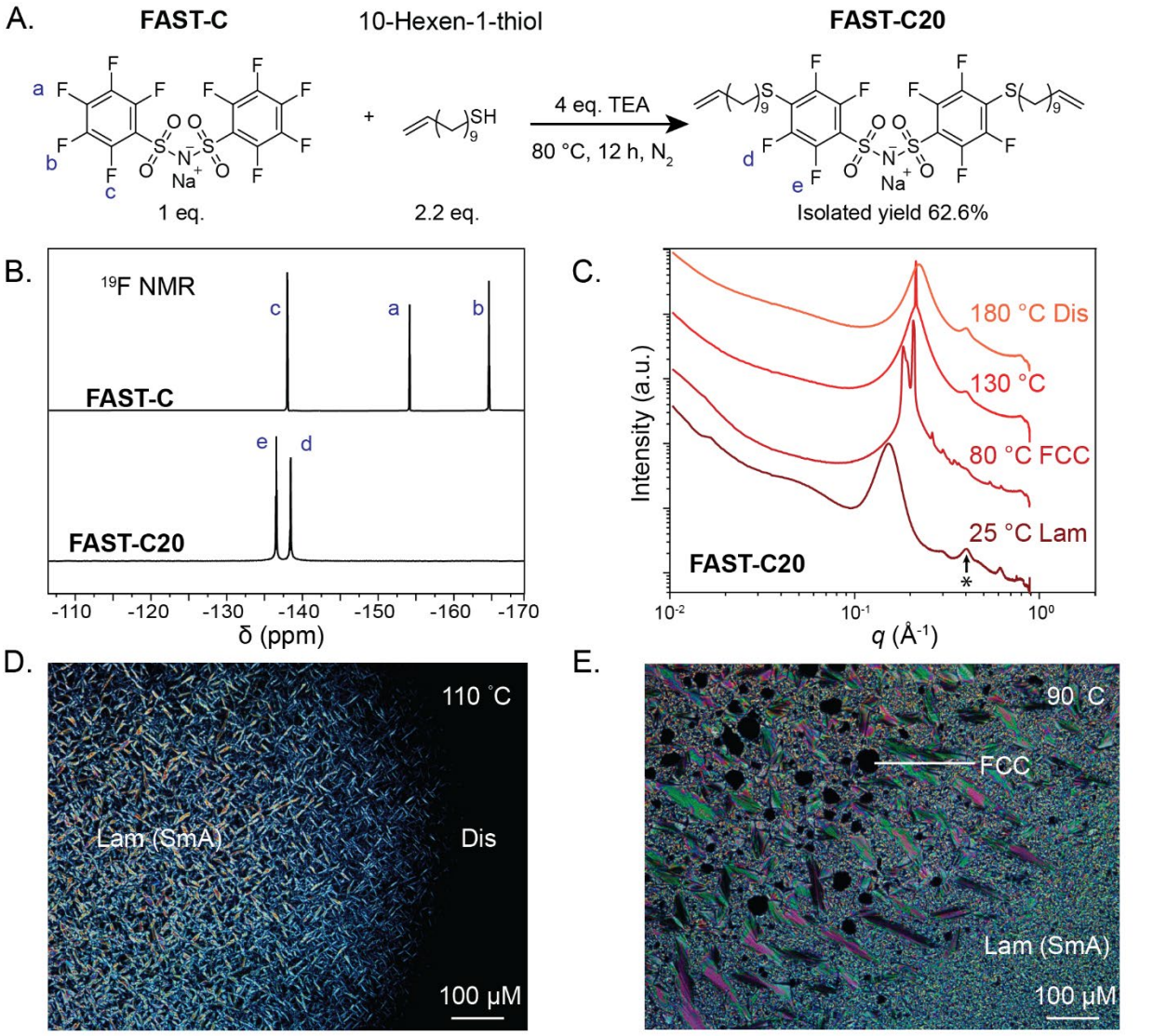

Figure 2. A) Scheme depicting the synthesis of monomer **FAST-C20**. B) ^{19}F Nuclear Magnetic Resonance (NMR) comparing **FAST-C** to **FAST-C20**. C). Small Angle X-Ray scattering (SAXS) showing the multiple ordered phases present for bulk **FAST-C20**. Peak patterns at 25, 80, and 180 °C were used to assign the phases as lamellar (Lam), face centered cubic (FCC), and disordered (isotropic) (Dis) respectively. The small peak at ~.4 Å^{-1} labeled with * is due to the Kapton window used during data acquisition. D and E) Polarized optical microscopy (POM) images of **FAST-C20**, showing the different liquid crystalline phases present. At 110 °C the appearance of bâtonnets indicates the nucleation of a smectic A (lamellar) phase from the disordered (isotropic) phase. As the temperature decreases to 90 °C the appearance of dark domains amongst the lamellar phase corresponds to the FCC phase identified by SAXS.

These results are consistent with **FAST-C20** behaving as a liquid crystal, which was further supported by polarized optical microscopy (POM, Figure 2D, E). At 110 °C (Figure 2D), which lies between the ordered FCC (80 °C) and mixed phases (130 °C) observed by SAXS, the nucleation of bâtonnets directly from the

isotropic phase, characteristic of a smectic A (SmA) liquid crystalline phase was observed.[30] The latter suggests that **FAST-C20** molecules are oriented in the same direction, with their long axis perpendicular to the layers. Upon cooling to 90 °C, dark domains appeared (Figure 2E) were assigned to FCC domains observed by SAXS, which are rotationally isotropic and, thus, inherently not birefringent. Upon cooling to 80 °C, most of the SmA phase receded and the POM textures appeared dark. Finally, the appearance of a second smectic phase was observed upon further cooling to 65 °C (Figure S6). As the two aryl rings form a hairpin in the **FAST-C** single crystal structure (Figure 1D), we propose that the internal angle between the two aryl rings can increase as a function of temperature resulting in the variety of liquid crystalline phases (Figure S7). Altogether, these POM results agree well with the VT-SAXS data, which suggest that **FAST-C20** has a high propensity to form ordered structures through nanoscale phase separation of its ionic and hydrocarbon segments, as observed for ionic liquid crystals.[31]

ADMET polymerization of FAST-C20 and cation exchange to provide a family of dissociative ionenes—pFAST-C20-M (where M = Na^+, Li^+, K^+, and Cs^+). Next, we focused on the polymerization of **FAST-C20** via ADMET. Initially, we explored common conditions for ADMET of non-ionic monomers, which involved refluxing a mixture of **FAST-C20** and Grubbs 1st-generation catalyst (1 mol %) in dichloromethane under nitrogen flow to remove ethylene;[32] however, poor solubility of the growing polymers in dichloromethane led to poor/inconsistent conversions. By contrast, conducting the polymerization in propylene carbonate and under vacuum (150 mTorr) to remove ethylene (Figure 3A) ensured solubility of the oligomeric intermediates and polymer products gave consistently high monomer conversions as determine by ^{1}H NMR (see supporting information for full details).[33] Upon quenching the reaction by addition of excess ethyl vinyl ether, the ionene product "**pFAST-C20-Na**" was isolated by precipitation into diethyl ether, filtration, and drying under vacuum at 180 °C for 12 hours. The number-average degree of polymerization, N_n, number-average molar mass, M_n, and *cis*/*trans* ratio of backbone alkenes of **pFAST-C20-Na** were estimated by ^{1}H NMR integration to be ~130, ~106 kDa, and 1:1.4, respectively (Figure 3B); the former values assume negligible cyclization. Additionally, no significant change was observed in the ^{19}F NMR spectra, indicating preservation of the tetrafluorinated aryl substituents (Figure S32). Size exclusion chromatography yielded a dispersity, $Đ$, of ~ 2, which is consistent with the step-growth nature of ADMET (Figure S39). Washing aliquots of **pFAST-C20-Na** with 1 M aqueous solutions of LiCl, KCl, or CsCl provided the Li^+, K^+, and Cs^+ analogs **pFAST-C20-Li**, **pFAST-C20-K**, and **pFAST-C20-Cs**, respectively, as confirmed by ^{7}Li,^{23}Na, and ^{133}Cs NMR, where appropriate (Figure S8). The cation exchanged ionenes were lyophilized to yield dry fluffy powders that were used for further study.

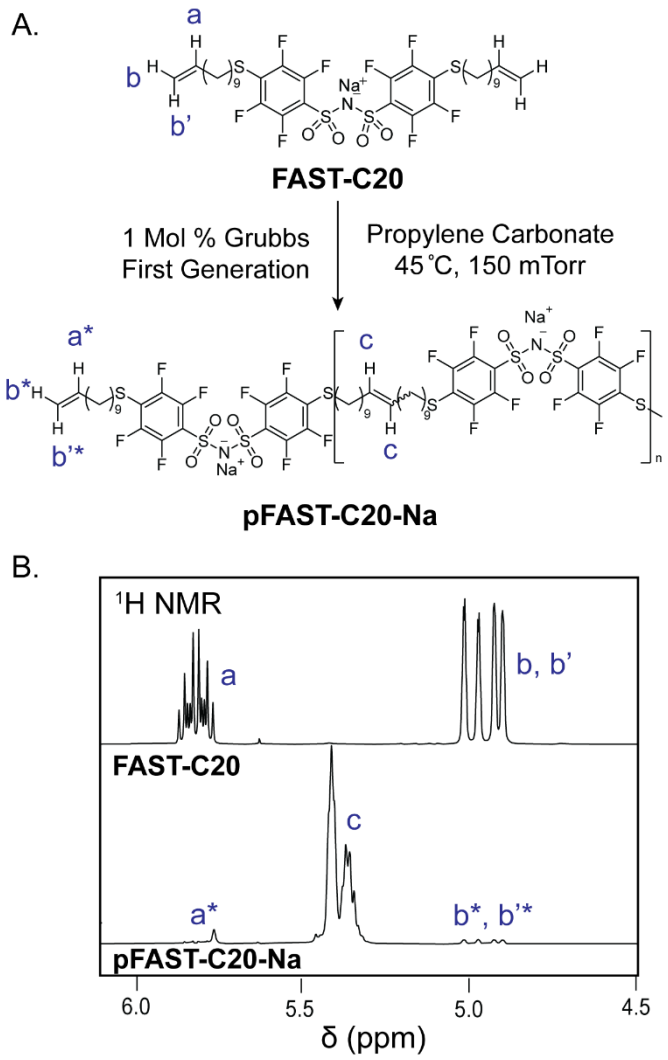

Figure 3. A) Synthesis of **pFAST-C20-Na** via ADMET polymerization of **FAST-C20**. The terminal protons of the **FAST-C20** (labeled as a, b, and b') become end groups (labeled as a*, b*, b'*) and internal alkenes (labeled c) in **pFAST-C20-Na**; integration of these peaks enables calculation of the number-average degree of polymerization and molar mass (neglecting cyclization). B) ^{1}H NMR spectra for **FAST-C20** (top) and **pFAST-C20-Na** (bottom) showing the relevant alkene resonances. The internal olefin (labeled as c) shows a mixture of *trans* and *cis* isomers as is expected for ADMET polymerization using Grubbs 1st-generation catalyst.[34] (600 MHz acetone-d_6, 25 °C).

Solid-state structural and thermal characterization of pFAST-C20-M polymers with various cations M. Films of each ionene were prepared by drop-casting from dilute solutions in DMF and drying under vacuum at 180 °C. VT-SAXS and VT-wide-angle X-ray scattering (VT-WAXS) (Figure 4A) curves displayed primary scattering peaks for each **pFAST-C20-M** polymer (q_1) at ~.15-.19 $Å^{-1}$ and higher-order reflections

at $2q_1$ and/or $3q_1$, consistent with a lamellar structure. The room-temperature SAXS pattern for **pFAST-C20-Na** showed a second peak, q_2, with higher-order reflections, indicative of a second lamellar domain, which can be attributed to lamellae at a different tilt angle as has been observed in other systems.[15] Peaks in the high q WAXS region (0.8-1.5 $Å^{-1}$) were observed for each sample, which are indicative of backbone crystallinity. Notably, the WAXS peaks of orthorhombic[8,16,26] or monoclinic polyethylene,[35] often observed for polymers with long alkyl spacers, are not observed for any of the polymers studied here, which may be due to the presence of *cis* and *trans* olefins in the polymer backbones and/or the sterically bulky FAST anions. In the future, hydrogenation of the polymer backbone could potentially be used to test these hypotheses.

Unlike monomer **FAST-C20**, which displayed multiple structural transitions as a function of temperature (Figure 2C), the lamellar morphology of each polymer was maintained up to at least 180 °C (Figure 4B, Figures S9–S12). **pFAST-C20-Li** was the only sample to show a significant change upon heating, displaying a shift to higher q and the emergence of a second set of peaks (q_2) with d_2 = 28.11 Å, indicative of a mixture of lamellar phases similar to those observed at room temperature for **pFAST-C20-Na.** These changes were reversible upon cooling to room temperature and waiting for ~5 days, suggesting that the single lamellar phase observed at room temperature is reasonably stable.

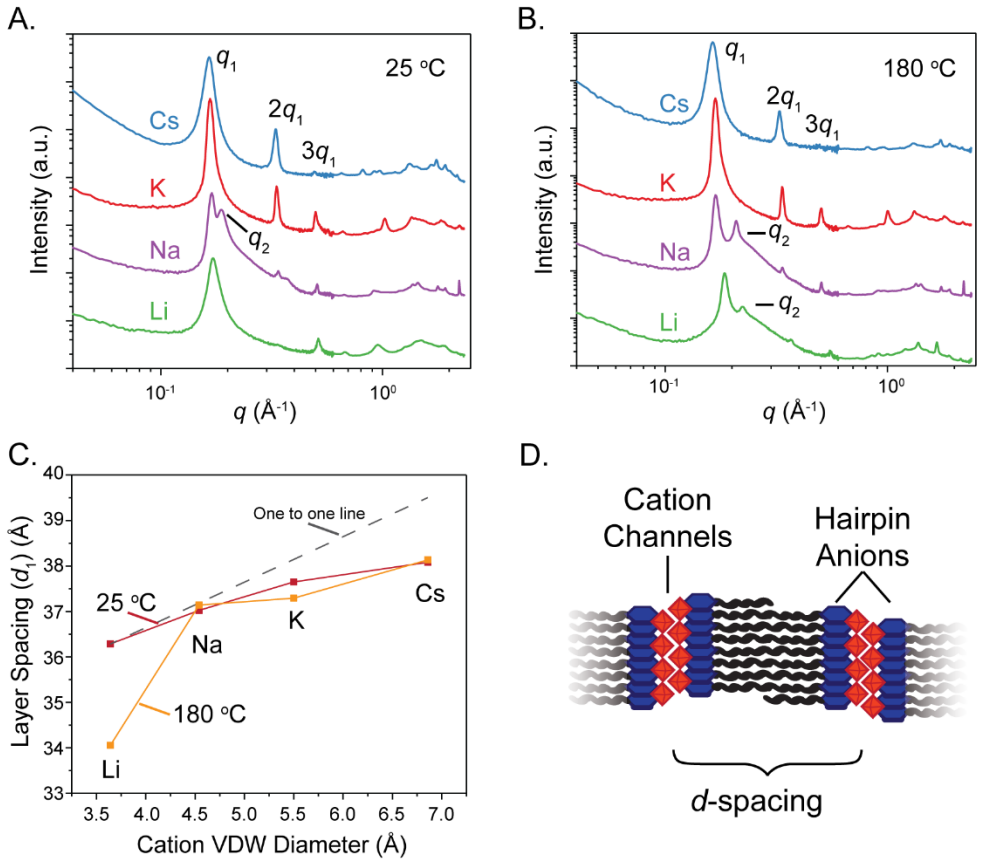

Figure 4. A and B) Reduced Small Angle X-Ray Scattering (SAXS) patterns of the 4 different variants of the **pFAST-C20-M** ionenes (M = Li, Na, K, and Cs) at 25 °C and 180 °C, respectively. The traces are offset for clarity and plotted on a log-log scale with intensity (a.u.) versus the scattering vector q (Å^{-1}). C) Real space dimensions (d-spacings) of the lamellae for each ionene versus the corresponding Van der Waals (VDW) diameter of the cation. As the cation size increases so does the size of the lamellae. D) Illustration of hypothesized lamellar structure of **pFAST-C20-M** ionenes based on X-ray scattering information and the single-crystal X-ray structure of **FAST-C** shown in Figure 1D. Cations are represented as red tetrahedra. Anions are represented as blue hexagons. Alkyl spacers are represented as black chains.

The d-spacings at room temperature and 180 °C for **pFAST-C20-M** increased with the Van der Waals diameters of the cations M (Figure 4C), which in consistent with a microstructure wherein the cations are sandwiched within anionic layers. The single-crystal X-ray structure of **FAST-C** (Figure 1D) similarly shows Na^+ ions sandwiched between layers of **FAST-C** anions with the perfluoroaryl rings of the latter folded away from the ion channels in hairpin structures, where the *para*-fluorine substituents are nearly parallel to each other. Thus, we propose that the solid-state structures of **pFAST-20C-M** polymers consist of layers of cations coordinated to hairpin-folded **FAST-C** anions (Figure 4D), each of which are linked to an adjacent layer by their *para*-C20 alkenyl segments. To further support for this proposed structure, we prepared

analogs of **pFAST-C20-M** with shorter, 10 carbon spacers between each anion (**pFAST-C10-M**), following similar procedures to those used above for **pFAST-C20-Na**. SAXS/WAXS characterization of **pFAST-C10-M** revealed similar lamellar structures compared to **pFAST-C20-M**, with *d* spacings that increase monotonically with the cation diameter (Figure S13). Notably, however, the **pFAST-C10-M** lamella were all ~10.5 Å smaller than the C20-M (Figure S14), regardless of cation size, supporting the notion that larger cations expand the ionic layers without impacting the alkenyl layers. Extrapolating these findings for **pFAST-C20-Na** and **pFAST-C10-Na** to a "zero carbon" spacer suggests that the ionic layers are ~13.1 Å thick, which agrees remarkably well with the observed distance—13.2 Å—between the *para*-carbon atoms of two **FAST-C** anions that span a single ionic layer in the crystal structure of **FAST-C** (Figure 1D; Figure S15).

Differential scanning calorimetry (DSC) was used to further investigate the thermal transitions in **pFAST-C20-M** (Table S1, Figure S15-S19). All of the ionenes, regardless of cation, showed endothermic transitions at >190 °C, which likely correlate to phase transitions in the lamellae or polymer backbone. In agreement with their VT-SAXS data, which displayed two sets of lamellae at 180 °C, **pFAST-C20-Li** and **pFAST-C20-Na** showed two endothermic transitions in the range of 180–260 °C. Additionally, glass transition temperatures were observed for **pFAST-C20-Li** and **pFAST-C20-Na** at ~ 100 °C, but were not detected for **pFAST-C20-K** and **pFAST-C20-Cs**, suggesting that the former may contain more amorphous domains in addition to the lamellae observed via SAXS. Finally, thermal gravimetric analysis (TGA) indicated that all of these ionenes were stable up to ~325 °C, with major degradation not occurring until >380 °C (Figure S20). Minimal (<4%) weight loss was observed before 325 °C, indicating the samples were dry.

Ionic conductivity of pFAST-C20-M ionenes. Given that **pFAST-C20-M** formed lamellar structures with cations sandwiched between anionic channels that are stable at high temperatures, we sought to characterize their ion conductivity. Figure 5A shows measured ionic conductivities versus inverse temperatures for the 4 different **pFAST-C20-M** ionenes. The conductivities span from ~10^{-8}–10^{-5} over the tested temperature range (80 to 180 °C, respectively) and are consistent and reversible over multiple cycles of heating and cooling between 80 and 180 °C (Figure S21; TableS1). While these conductivities are ~2–3 orders-of-magnitude lower than optimized SPEs that depend on segmental motion (e.g., PEO-based SPEs), the observations of linear conductivity versus 1000/T profiles for 3 of the 4 ionenes (**pFAST-C20-Na**, **pFAST-C20-Li**, and **pFAST-C20-K**) and reasonable conductivity well below T_m and T_g (including conductivity ~7–8 orders-of-magnitude greater that coupled SPEs at T_g) are consistent with a decoupled

ion conduction mechanism for these samples.[11] These data can thus be fitted with an Arrhenius equation of the form:

$$\textbf{Equation 1: } \sigma = \sigma_0 * exp(^{-E_a}/_{RT})$$

Where E_a is the activation energy of ionic transport in kJ/mol, σ_0 is a pre-exponential factor, R is the universal gas constant, and T is temperature (Figure S19). Interestingly, **pFAST-C20-Li** and **pFAST-C20-Na** were found to have similar activation energies of 59 and 60 kJ/mol, respectively. **PFAST-C20-K** displayed a higher activation energy of 70 kJ/mol, but overall greater ionic conductivity at all temperatures. While other works have suggested that larger, softer cations have lower activation energies for ionic transport,[16,17] for **pFAST-C20-M**, confinement of the cations to the ionic channels may impede hopping of larger cations. We note that the curvature in the conductivity versus 1/T plot for **pFAST-C20-Cs** suggests that these data are better fitted with the Vogell-Fulcher-Tammann (VTF) equation that is typically used for coupled SPEs (see supporting information for details). Thus, we do not focus on this sample in the remaining discussion.

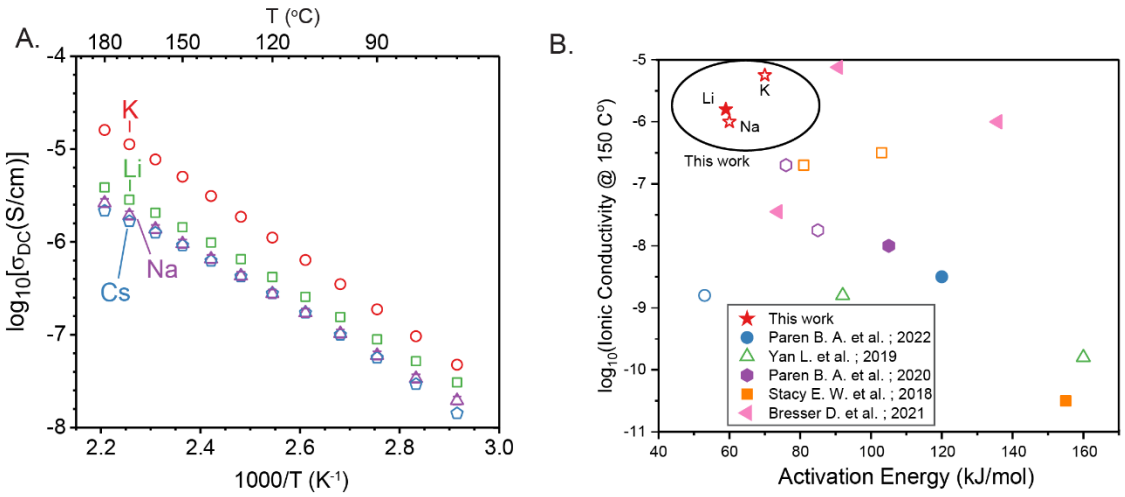

Figure 5. A) Variable temperature ion conductivities of **pFAST-C20-M** ionenes with varied cations M. B) Comparisons of the activation energies and ionic conductivities at 150 °C for this work and reported solvent-free ionenes and ionomers (references 21–25) where Arrhenius activation energies are provided. Solid markers denote Li^+ variants of the respective ionomer/ionene, while the hollow points include Na^+, K^+, and Cs^+ variants. Detailed structures from each reference are provided in Figure S20.

It is notable that the fitted Arrhenius activation energies for **pFAST-C20-Li**, **pFAST-C20-Na**, and **pFAST-C20-K** are amongst the lowest reported for dry ionene/ionomer conductors that are proposed to operate via a decoupled ion conduction mechanism (Figure 5B; see Figure S22 for structures of each referenced

example). Similar, the ionic conductivities at 150 °C for our ionenes are amongst the highest of related systems. We proposed that this performance is directly related to the highly dissociative **FAST-C** molecular structure (Figure 1), demonstrating that molecular design at the level of anionic substituents in ionene conductors may provide a path toward optimal SPEs in the future.

Investigating the mechanism of ion conduction using nudged elastic band calculations. To gain further insight into the potential ion conduction mechanisms in these **pFAST-C20-M** ionenes, nudged elastic band (NEB) calculations were performed using the **FAST-C** crystal structure (Figure 1D) as a model and assuming that the ionic channels within bulk **pFAST-C20-M** ionenes have similar local structures (see supplementary section S3; Figures S25–29). Two ion-hopping mechanisms were explored: vacancy mediated and concerted. For the Li^+ ionene, both mechanisms had similar calculated energy barriers (~68 kJ/mol) and agreed well with the experimentally measured activation energy (~60 kJ/mol), suggesting that either may be operative in **pFAST-C20-Li**. For Na^+ and K^+ ionenes, the vacancy-mediated mechanism gave significantly lower calculated energy barriers (~70 kJ/mol versus 112 kJ/mol for vacancy-mediated and concerted mechanisms for Na^+, respectively), the former of which were consistent with the experimentally determined barriers of ~70 kJ/mol. These results suggest that stoichiometric imbalances, perhaps created at disordered interfaces or boundaries between crystalline domains as established for ceramic conductors,[36–38] may be advantageous to ion conduction in these ionenes. NEB calculations also indicated that the highest energy structure for each ion-hopping trajectory corresponded with loss of an oxygen ligand from adjacent **FAST-C** anions (See S26–29), suggesting that further molecular engineering of the anion structure, perhaps via *ortho*-substitution to introduce additional weakly coordinating ligands, may provide a path toward even lower energy barriers.

Selective cation solvation leads to significant ion conductivity improvement in ionene SPEs. Given the well-defined anionic channels in **pFAST-C20-M**, we wondered if it would be possible to add a small amount of cation-coordinating solvent to further increase conductivity through those channels without disrupting their overall lamellar structure.[39] We were particularly inspired by Solvate Ionic liquids (SILs), which are a class of ionic liquids wherein strongly binding solvents form supramolecular solvent–cation complexes with virtually no "bulk" solvent.[40] This unique structure facilitates anion dissociation and can lead to improved ionic conductivity, low vapor pressure, and excellent electrochemical stability.[40,41] SIL formation requires highly dissociative anions such as TFSI; given the highly dissociative nature of **FAST-C**, and our previous finding that *para*-thioether-functionalized fluorinated aryl sulfonamide salts similar to **FAST-C**

form SILs in the presence of 1 equiv tetraglyme (G4),[24] we hypothesized that it may be possible facilitate the formation of SIL-like cation complexes within the channels of **pFAST-C20-Li** using G4 solvent.

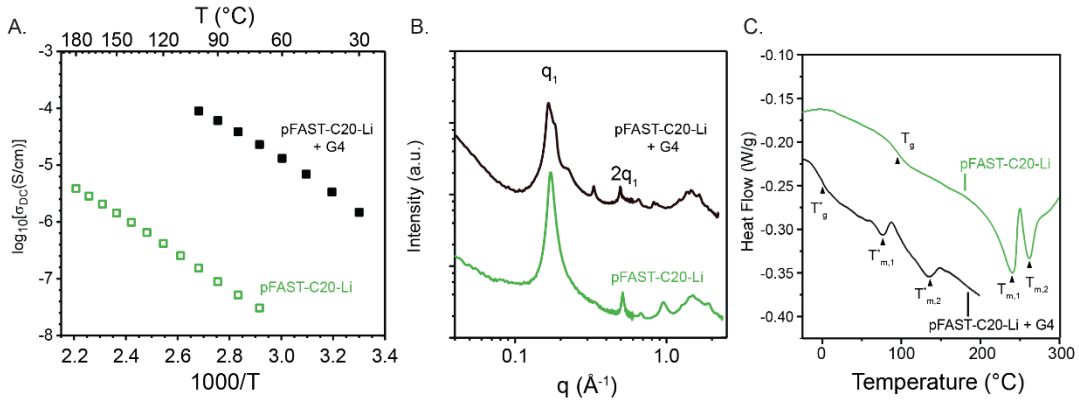

Figure 6. A) Ionic conductivities of **pFAST-C20-Li** and **pFAST-C20-Li** + G4 (1 equiv per cation). B) 1D SAXS and WAXS profiles **pFAST-C20-Li** and **pFAST-C20-Li** + G4**,** showing that the ordered lamellar structure is retained upon G4 addition with slight changes in the shape of the primary peak q_1 and in the high q region (>1.0 Å^{-1}). C) DSC traces (from the second heating cycle) for **pFAST-C20-Li** and **pFAST-C20-Li** + G4.

In support of our hypothesis, we observed significant increases in conductivity for **pFAST-20-Li** after exposure to 1 equiv of G4 (Figure 6a). For example, at 80 °C, the ionic conductivity of **pFAST-20-Li** + G4 was ~3 orders-of-magnitude greater than dry **pFAST-20-Li**. Fitting the conductivity data (Figure S23; Table S2) for **pFAST-20-Li** + G4 revealed a similar activation energy but a ~1000-fold larger pre-factor compared to dry **pFAST-20-Li**, suggesting that solvation leads to a larger number of mobile cations. Notably, VT-SAXS and VT-WAXS analysis (Figure 6B; Figure S24) suggested that the G4-containing material maintained a highly ordered lamellar structure with scattering peaks at q_1 = .166 Å^{-1}, $2q_1$, and $3q_1$ till at least 100 °C. Moreover, the lamellar *d*-spacing for **pFAST-20-Li + G4** (35.7 Å) was greater than that for dry **pFAST-C20-Li** (33.4 Å) by 2.3 Å, which is within the expected size difference of reported Li^+ coordinated by G4 or crown ethers compared to Li+ alone.[42,43] DSC analysis (Figure 6C) showed T_g and T_m transitions for **pFAST-C20-Li** + G4 that were >100 °C lower than for the dry ionene, indicative of plasticization, which is expected to increase ion conductivity. Finally, crystallization of G4 (T_c = – 9.4 °C)[44] was not observed, suggesting that the presence of minimal bulk G4.

Conclusions. Here, we introduce the concept of using highly dissociative, electron deficient anions as building blocks for ionene synthesis. Specifically, the symmetrical **FAST-C** anion that is highly dissociative, easily functionalizable via S_NAr, and capable of forming channel structures in the solid state was leveraged to generate a new diene monomer **FAST-C20** for ADMET polymerization. **FAST-C20** showed a high

propensity to self-assemble on its own, forming multiple different thermally responsive liquid crystalline phases. After polymerization, the resulting ionenes—**pFAST-C20-M**— form highly ordered lamellar bulk materials driven by Van der Waals interactions of the C20 linkers and aggregation of the anionic **FAST-C** domains. Due to their highly ordered structures and dissociative anions, **pFAST-C20-M** polymers display amongst the highest overall ionic conductivities and lowest activation energies for ion conduction reported for dry polymer electrolytes proposed to operate via cation hopping. Furthermore, we show that cation solvation can be achieved without significant disruption to the overall lamellar structure, resulting in a ~three orders-of-magnitude increase to ionic conductivity. This work suggests that anion molecular design may offer a path to further improve the performance of decoupled solid polymer electrolytes. Looking forward, inspiration can be drawn from the ceramic ion conductor field, where vacancy assisted diffusion plays a key role in ion conduction, and large gains in ionic conductivity can be achieved by aliovalent doping.[45] Additionally, through future monomer designs, geometric connectivity and distances between anionic hopping sites can be tuned to further improve ionic conductivities and lower activation energies.[13] We expect that novel, highly dissociative anionic building blocks will be key to these endeavors.

References.

(1) Hallinan, D. T.; Balsara, N. P. Polymer Electrolytes. *Annu Rev Mater Res* **2013**, *43* (1), 503–525. https://doi.org/10.1146/annurev-matsci-071312-121705.

(2) Xue, Z.; He, D.; Xie, X. Poly(Ethylene Oxide)-Based Electrolytes for Lithium-Ion Batteries. *Journal of Materials Chemistry A*. Royal Society of Chemistry July 17, 2015, pp 19218–19253. https://doi.org/10.1039/c5ta03471j.

(3) Zhang, H.; Li, C.; Piszcz, M.; Coya, E.; Rojo, T.; Rodriguez-Martinez, L. M.; Armand, M.; Zhou, Z. Single Lithium-Ion Conducting Solid Polymer Electrolytes: Advances and Perspectives. *Chem Soc Rev* **2017**, *46* (3), 797–815. https://doi.org/10.1039/C6CS00491A.

(4) Doyle, M.; Fuller, T. F.; Newman, J. The Importance of the Lithium Ion Transference Number in Lithium/Polymer Cells. *Electrochim Acta* **1994**, *39* (13), 2073–2081. https://doi.org/10.1016/0013-4686(94)85091-7.

(5) Thomas, K. E.; Sloop, S. E.; Kerr, J. B.; Newman, J. Comparison of Lithium-Polymer Cell Performance with Unity and Nonunity Transference Numbers. *J Power Sources* **2000**, *89* (2), 132–138. https://doi.org/10.1016/S0378-7753(00)00420-1.

(6) Li, S.; Mohamed, A. I.; Pande, V.; Wang, H.; Cuthbert, J.; Pan, X.; He, H.; Wang, Z.; Viswanathan, V.; Whitacre, J. F.; Matyjaszewski, K. Single-Ion Homopolymer Electrolytes with High

Transference Number Prepared by Click Chemistry and Photoinduced Metal-Free Atom-Transfer Radical Polymerization. *ACS Energy Lett* **2018**, *3* (1), 20–27. https://doi.org/10.1021/acsenergylett.7b00999.

(7) Dewing, B. L.; Bible, N. G.; Ellison, C. J.; Mahanthappa, M. K. Electrochemically Stable, High Transference Number Lithium Bis(Malonato)Borate Polymer Solution Electrolytes. *Chemistry of Materials* **2020**, acs.chemmater.9b05219. https://doi.org/10.1021/acs.chemmater.9b05219.

(8) Park, J.; Staiger, A.; Mecking, S.; Winey, K. I. Enhanced Li-Ion Transport through Selectively Solvated Ionic Layers of Single-Ion Conducting Multiblock Copolymers. *ACS Macro Lett* **2022**, 1008–1013. https://doi.org/10.1021/ACSMACROLETT.2C00288.

(9) Zhang, W.; Feng, S.; Huang, M.; Qiao, B.; Shigenobu, K.; Giordano, L.; Lopez, J.; Tatara, R.; Ueno, K.; Dokko, K.; Watanabe, M.; Shao-Horn, Y.; Johnson, J. A. Molecularly Tunable Polyanions for Single-Ion Conductors and Poly(Solvate Ionic Liquids). *Chemistry of Materials* **2021**, *33* (2), 524–534. https://doi.org/10.1021/ACS.CHEMMATER.0C03258/ASSET/IMAGES/MEDIUM/CM0C03258_M006.GIF.

(10) Elmore, C.; Seidler, M.; Ford, H.; Merrill, L.; Upadhyay, S.; Schneider, W.; Schaefer, J. Ion Transport in Solvent-Free, Crosslinked, Single-Ion Conducting Polymer Electrolytes for Post-Lithium Ion Batteries. *Batteries* **2018**, *4* (2), 28. https://doi.org/10.3390/batteries4020028.

(11) Bocharova, V.; Sokolov, A. P. Perspectives for Polymer Electrolytes: A View from Fundamentals of Ionic Conductivity. *Macromolecules* **2020**, *53* (11), 4141–4157. https://doi.org/10.1021/ACS.MACROMOL.9B02742/ASSET/IMAGES/LARGE/MA9B02742_0002.JPEG.

(12) Gao, J.; Wang, C.; Han, D. W.; Shin, D. M. Single-Ion Conducting Polymer Electrolytes as a Key Jigsaw Piece for next-Generation Battery Applications. *Chem Sci* **2021**, *12* (40), 13248–13272. https://doi.org/10.1039/D1SC04023E.

(13) Bachman, J. C.; Muy, S.; Grimaud, A.; Chang, H. H.; Pour, N.; Lux, S. F.; Paschos, O.; Maglia, F.; Lupart, S.; Lamp, P.; Giordano, L.; Shao-Horn, Y. Inorganic Solid-State Electrolytes for Lithium Batteries: Mechanisms and Properties Governing Ion Conduction. *Chem Rev* **2016**, *116* (1), 140–162. https://doi.org/10.1021/ACS.CHEMREV.5B00563/ASSET/IMAGES/LARGE/CR-2015-005635_0025.JPEG.

(14) Krauskopf, T.; Muy, S.; Culver, S. P.; Ohno, S.; Delaire, O.; Shao-Horn, Y.; Zeier, W. G. Comparing the Descriptors for Investigating the Influence of Lattice Dynamics on Ionic Transport Using the Superionic Conductor $Na_3PS_{4-x}Se_x$. *J Am Chem Soc* **2018**, *140* (43), 14464–14473. https://doi.org/10.1021/jacs.8b09340.

(15) Yan, L.; Häußler, M.; Bauer, J.; Mecking, S.; Winey, K. I. Monodisperse and Telechelic Polyethylenes Form Extended Chain Crystals with Ionic Layers. *Macromolecules* **2019**, *52* (13), 4949–4956. https://doi.org/10.1021/acs.macromol.9b00962.

(16) Paren, B. A.; Häußler, M.; Rathenow, P.; Mecking, S.; Winey, K. I. Decoupled Cation Transport within Layered Assemblies in Sulfonated and Crystalline Telechelic Polyethylenes.

Macromolecules **2022**, *55* (7), 2813–2820. https://doi.org/10.1021/ACS.MACROMOL.2C00132/ASSET/IMAGES/MEDIUM/MA2C00132_M001.GIF.

(17) Paren, B. A.; Thurston, B. A.; Neary, W. J.; Kendrick, A.; Kennemur, J. G.; Stevens, M. J.; Frischknecht, A. L.; Winey, K. I. Percolated Ionic Aggregate Morphologies and Decoupled Ion Transport in Precise Sulfonated Polymers Synthesized by Ring-Opening Metathesis Polymerization. *Macromolecules* **2020**, *53* (20), 8960–8973. https://doi.org/10.1021/ACS.MACROMOL.0C01906/ASSET/IMAGES/LARGE/MA0C01906_0011.JPEG.

(18) Bresser, D.; Leclere, M.; Bernard, L.; Rannou, P.; Mendil-Jakani, H.; Kim, G. T.; Zinkevich, T.; Indris, S.; Gebel, G.; Lyonnard, S.; Picard, L. Organic Liquid Crystals as Single-Ion Li+ Conductors. *ChemSusChem* **2021**, *14* (2), 655–661. https://doi.org/10.1002/cssc.202001995.

(19) Stacy, E. W.; Gainaru, C. P.; Gobet, M.; Wojnarowska, Z.; Bocharova, V.; Greenbaum, S. G.; Sokolov, A. P. Fundamental Limitations of Ionic Conductivity in Polymerized Ionic Liquids. *Macromolecules* **2018**, *51* (21), 8637–8645. https://doi.org/10.1021/ACS.MACROMOL.8B01221/ASSET/IMAGES/MEDIUM/MA-2018-012217_M010.GIF.

(20) Bresser, D.; Lyonnard, S.; Iojoiu, C.; Picard, L.; Passerini, S. Decoupling Segmental Relaxation and Ionic Conductivity for Lithium-Ion Polymer Electrolytes. *Molecular Systems Design and Engineering*. Royal Society of Chemistry August 1, 2019, pp 779–792. https://doi.org/10.1039/c9me00038k.

(21) Xu, K. Nonaqueous Liquid Electrolytes for Lithium-Based Rechargeable Batteries. *Chem Rev* **2004**, *104* (10), 4303–4417. https://doi.org/10.1021/CR030203G/ASSET/IMAGES/LARGE/CR030203GH00012.JPEG.

(22) Mc Naught, a. D.; Wilkinson, a. Compendium of Chemical Terminology-Gold Book. *Iupac* **2012**, 1670. https://doi.org/10.1351/goldbook.

(23) Huang, M.; Feng, S.; Zhang, W.; Giordano, L.; Chen, M.; Amanchukwu, C. v.; Anandakathir, R.; Shao-Horn, Y.; Johnson, J. A. Fluorinated Aryl Sulfonimide Tagged (FAST) Salts: Modular Synthesis and Structure–Property Relationships for Battery Applications. *Energy Environ Sci* **2018**, *11* (5), 1326–1334. https://doi.org/10.1039/C7EE03509H.

(24) Huang, M.; Feng, S.; Zhang, W.; Lopez, J.; Qiao, B.; Tatara, R.; Giordano, L.; Shao-Horn, Y.; Johnson, J. A. Design of S-Substituted Fluorinated Aryl Sulfonamide-Tagged (S-FAST) Anions to Enable New Solvate Ionic Liquids for Battery Applications. *Chemistry of Materials* **2019**, *31* (18), 7558–7564. https://doi.org/10.1021/acs.chemmater.9b02353.

(25) Trigg, E. B.; Winey, K. I. Nanoscale Layers in Polymers to Promote Ion Transport. *Mol Syst Des Eng* **2019**, *4* (2), 252–262. https://doi.org/10.1039/C8ME00086G.

(26) Trigg, E. B.; Gaines, T. W.; Maréchal, M.; Moed, D. E.; Rannou, P.; Wagener, K. B.; Stevens, M. J.; Winey, K. I. Self-Assembled Highly Ordered Acid Layers in Precisely Sulfonated Polyethylene

Produce Efficient Proton Transport. *Nat Mater* **2018**, *17* (8), 725–731. https://doi.org/10.1038/s41563-018-0097-2.

(27) Rosen, B. M.; Wilson, C. J.; Wilson, D. A.; Peterca, M.; Imam, M. R.; Percec, V. Dendron-Mediated Self-Assembly, Disassembly, and Self-Organization of Complex Systems. *Chem Rev* **2009**, *109* (11), 6275–6540. https://doi.org/10.1021/CR900157Q/ASSET/IMAGES/CR-2009-00157Q_M025.GIF.

(28) Impéror-Clerc, M. Thermotropic Cubic Mesophases. *Current Opinion in Colloid and Interface Science*. Elsevier June 1, 2005, pp 370–376. https://doi.org/10.1016/j.cocis.2004.12.004.

(29) Balagurusamy, V. S. K.; Ungar, G.; Percec, V.; Johansson, G. Rational Design of the First Spherical Supramolecular Dendrimers Self-Organized in a Novel Thermotropic Cubic Liquid-Crystalline Phase and the Determination of Their Shape by X-Ray Analysis. *J Am Chem Soc* **1997**, *119* (7), 1539–1555. https://doi.org/10.1021/ja963295i.

(30) Dierking, I. Textures of Liquid Crystals. *Textures of Liquid Crystals* **2003**. https://doi.org/10.1002/3527602054.

(31) Goossens, K.; Lava, K.; Bielawski, C. W.; Binnemans, K. Ionic Liquid Crystals: Versatile Materials. **2016**. https://doi.org/10.1021/cr400334b.

(32) Gaines, T. W.; Bell, M. H.; Trigg, E. B.; Winey, K. I.; Wagener, K. B. Precision Sulfonic Acid Polyolefins via Heterogenous to Homogenous Deprotection. *Macromol Chem Phys* **2018**, *219* (11), 1700634. https://doi.org/10.1002/macp.201700634.

(33) Lucero, J. M.; Romero, Z.; Moreno, A.; Huber, D. L.; Simocko, C. ADMET Polymerization in Affordable, Commercially Available, High Boiling Solvents. *SN Appl Sci* **2020**, *2* (4), 1–8. https://doi.org/10.1007/S42452-020-2385-0/TABLES/2.

(34) Schulz, M. D.; Wagener, K. B.; Schulz, M. D.; Wagener The George, K. B.; Butler, J. Precision Polymers through ADMET Polymerization. *Macromol Chem Phys* **2014**, *215* (20), 1936–1945. https://doi.org/10.1002/MACP.201400268.

(35) Russell, K. E.; Hunter, B. K.; Heyding, R. D. *Monoclinic Polyethylene Revisited*; 1997; Vol. 38.

(36) Alexander, K. C.; Ganesh, P.; Chi, M.; Kent, P.; Sumpter, B. G. Grain Boundary Stability and Influence on Ionic Conductivity in a Disordered Perovskite—a First-Principles Investigation of Lithium Lanthanum Titanate. *MRS Commun* **2016**, *6* (4), 455–463. https://doi.org/10.1557/MRC.2016.58.

(37) Peters, A.; Korte, C.; Hesse, D.; Zakharov, N.; Janek, J. Ionic Conductivity and Activation Energy for Oxygen Ion Transport in Superlattices — The Multilayer System CSZ (ZrO2 + CaO) / Al2O3. *Solid State Ion* **2007**, *178* (1–2), 67–76. https://doi.org/10.1016/J.SSI.2006.12.004.

(38) He, X.; Sun, H.; Ding, X.; Zhao, K. Grain Boundaries and Their Impact on Li Kinetics in Layered-Oxide Cathodes for Li-Ion Batteries. *Journal of Physical Chemistry C* **2021**, *125* (19), 10284–10294. https://doi.org/10.1021/ACS.JPCC.1C02400/ASSET/IMAGES/LARGE/JP1C02400_0006.JPEG.

(39) Ue, M.; Mori, S. *Mobility and Ionic Association of Lithium Salts in a Propylene Carbonate-Ethyl Methyl Carbonate Mixed Solvent*; 1995.

(40) Mandai, T.; Yoshida, K.; Ueno, K.; Dokko, K.; Watanabe, M. Criteria for Solvate Ionic Liquids. *Physical Chemistry Chemical Physics* **2014**, *16* (19), 8761–8772. https://doi.org/10.1039/C4CP00461B.

(41) Mandai, T.; Dokko, K.; Watanabe, M. Solvate Ionic Liquids for Li, Na, K, and Mg Batteries. *The Chemical Record* **2019**, *19* (4), 708–722. https://doi.org/10.1002/TCR.201800111.

(42) Henderson, W. A.; Brooks, N. R.; Young, V. G. Tetraglyme-Li+ Cation Solvate Structures: Models for Amorphous Concentrated Liquid and Polymer Electrolytes (II). *Chemistry of Materials* **2003**, *15* (24), 4685–4690. https://doi.org/10.1021/CM034352R/SUPPL_FILE/CM034352RSI20030513_110601.PDF.

(43) Ichihashi, K.; Konno, D.; Date, T.; Nishimura, T.; Maryunina, K. Y.; Inoue, K.; Nakaya, T.; Toyoda, K.; Tatewaki, Y.; Akutagawa, T.; Nakamura, T.; Nishihara, S. Optimizing Lithium Ion Conduction through Crown Ether-Based Cylindrical Channels in [Ni(Dmit)2]- Salts. *Chemistry of Materials* **2018**, *30* (20), 7130–7137. https://doi.org/10.1021/ACS.CHEMMATER.8B03027/SUPPL_FILE/CM8B03027_SI_002.CIF.

(44) *CRC Handbook of Chemistry and Physics 103rd Edition*. CRC Press. https://hbcp.chemnetbase.com/faces/contents/InteractiveTable.xhtml (accessed 2023-04-11).

(45) Zhang, Z.; Shao, Y.; Lotsch, B.; Hu, Y. S.; Li, H.; Janek, J.; Nazar, L. F.; Nan, C. W.; Maier, J.; Armand, M.; Chen, L. New Horizons for Inorganic Solid State Ion Conductors. *Energy Environ Sci* **2018**, *11* (8), 1945–1976. https://doi.org/10.1039/C8EE01053F.

FOR TABLE OF CONTENTS ONLY: